A DFT and ab initio direct dynamics study on the hydrogen abstract reaction of H3BNH3 → H2 + H2BNH2

ARTICLE *in* CHEMICAL PHYSICS LETTERS · MARCH 2005

Impact Factor: 1.9 · DOI: 10.1016/j.cplett.2005.01.024

3 AUTHORS, INCLUDING:

Jian-Guo Zhang
Beijing Institute of Technology
312 PUBLICATIONS **1,577** CITATIONS

Available online at www.sciencedirect.com
SCIENCE DIRECT®
Chemical Physics Letters 404 (2005) 100–106
CHEMICAL PHYSICS LETTERS
www.elsevier.com/locate/cplett

A DFT and ab initio direct dynamics study on the hydrogen abstract reaction of $H_3BNH_3 \rightarrow H_2 + H_2BNH_2$

Qian Shu Li *, Jianguo Zhang [1], Shaowen Zhang *

State Key Laboratory of Prevention and Control of Explosion Disasters and School of Science, Beijing Institute of Technology, Beijing 100081, PR China

Received 14 December 2004

Abstract

A direct ab initio dynamics study is presented on the hydrogen abstraction reaction of $H_3BNH_3 \rightarrow H_2 + H2BNH_2$. The geometries of all the stationary points are optimized at the B3LYP and MP2 levels of theory with a series of basis sets up to aug-cc-pVTZ. The energies are refined using the G3, G3MP2, G3MP2B3, CBS-Q, CBS-Q//B3, and a combined high-level (HL) method based on the geometries optimized using the B3LYP/aug-cc-pVTZ level of theory. The rate constants are evaluated using the conventional transition-state theory and canonical variational transition-state theory (CVT). The fitted Arrhenius expression calculated from the CVT/SCT method is $k(T) = 6.86 \times 10^6 \times T^{1.69} \times e^{(-1.37\times10^4/T)}$ s^{-1}. The estimated apparent activation energy is in accordance with experimental results.

1. Introduction

Recent experiments have shown that ammonia-borane (H_3BNH_3) can decompose at relatively low temperatures (below 410 K) accompanied by heat evolution and hydrogen release. This character and its relatively high hydrogen content (about 20 mass percent) allow H_3BNH_3 to be a potential compound as chemical hydrogen (H_2) storage medium for fuel cell and other applications [1–5]. The knowledge of mechanism and dynamics of the thermal decomposition process of H_3BNH_3 is helpful for these applications and has attracted the interests of many experimental chemists [1–6].

In 1985, Geanangel and Wendlandt [3] described the process of three stepwise hydrogen loss from H_3BNH_3 to BN by the thermogravimetry (TG) and differential scanning calorimetry (DSC) technologies. Then, Sit et al. [4] suggested the thermal dissociation mechanism of H_3BNH_3 by differential thermal analysis (DTA) curves at different heating rates of 2, 5 and 10 K/min in a dynamic N_2, which better define the chemical steps in the decomposition reaction. Recently, Wolf and co-workers [1,2] investigated the thermally activated decomposition of H_3BNH_3 by using the combined thermo-analytical methods, which indicated that H_3BNH_3 undergoes stepwise thermal decomposition in the temperature range up to 500 K. They found that H_3BNH_3 is already decomposed at 410 K. The reaction enthalpy is about -5.19 ± 0.48 kcal/mol at different heating rates and temperatures by using the DSC technology. During the first decomposition step, H_3BNH_3 releases approximately 1 mol H_2 per mol H_3BNH_3. The other decomposition products are aminoborane (H_2BNH_2), polymeric aminoborane $(H_2BNH_2)_x$ and a small amount of the volatile borazine $B_3N_3H_6$. The H_2BNH_2 was characterized by elemental analysis, IR-spectroscopy and X-ray powder diffraction measurements. These experimental results indicate that H_3BNH_3 can decompose to

* Corresponding authors. Fax: +86 10 68912665.
E-mail addresses: qsli@bit.edu.cn (Q.S. Li), zjgbit@sina.com (J. Zhang).
[1] Fax: +86 10 6891 1202.

0009-2614/$ - see front matter © 2005 Elsevier B.V. All rights reserved.
doi:10.1016/j.cplett.2005.01.024

H_2BNH_2 and a hydrogen molecule with a relatively low reaction barrier. However, according to the best of our knowledge, both the energetic information and kinetics data for this reaction are quite limited.

In the present study, we provide a dynamics study on the H_2 elimination reaction of H_3BNH_3 by employing the direct ab initio dynamics method [7]. The energetic of the reaction is calculated using high-level quantum mechanics methods and the rate constants are calculated using the canonical variational transition-state theory with small curvature tunneling correction.

2. Methodology

2.1. Electronic structure calculations

The geometries and frequencies of all stationary points (reactants, products, and the transition state) are optimized using the B3LYP and MP2 methods with the cc-pVDZ, aug-cc-pVDZ, cc-pVTZ and aug-cc-pVTZ basis sets [8]. Here, B3LYP [9] denotes the combination of the Becke's three-parameter exchange functional with the Lee–Yang–Parr (LYP) [10] correlation functional. To yield more reliable reaction enthalpy and barrier, the energies of all stationary points are further refined with several multi-level methods such as the G3 [11], G3MP2 [12], G3MP2B3 [13], CBS-Q [14], CBS-Q//B3 [15], and a combined high-level method suggested by Martin [16] (denoted as HL) based on the optimized geometries at the B3LYP/aug-cc-pVTZ levels of theory. Here, the HL method employs a combination of quadratic configuration interaction calculations with perturbative inclusion of the triplet contribution, QCISD(T) [17], and second-order Møller–Plesset perturbation theory (MP2) [18]. It estimates the infinite basis set limit via the extrapolation of results obtained from sequences of the correlation-consistent polarized-valence basis sets. The higher-level estimate, E_{HL}, is obtained as the sum of the QCISD(T) extrapolations. The combination of extrapolations can be expressed as [16]:

$$\begin{aligned} E_{HL} = {} & \mathrm{E[QCISD(T)/cc\text{-}pVTZ]} \\ & + \{\mathrm{E[QCISD(T)/cc\text{-}pVTZ]} \\ & - \mathrm{E[QCISD(T)/cc\text{-}pVDZ]}\} \times 0.46286 \\ & + \mathrm{E[MP2/cc\text{-}pVQZ]} + \{\mathrm{E[MP2/cc\text{-}pVQZ]} \\ & - \mathrm{E[MP2/cc\text{-}pVTZ]}\} \times 0.69377 \\ & + \mathrm{E[MP2/cc\text{-}pVTZ]} + \{\mathrm{E[MP2/cc\text{-}pVTZ]} \\ & - \mathrm{E[MP2/cc\text{-}pVDZ]}\} \times 0.46286 \end{aligned}$$

The minimum energy path (MEP) is obtained using the intrinsic reaction coordinate (IRC) method [19] at the B3LYP/aug-cc-pVTZ level of theory. In the calculation of rate constants, the energies of points on the MEP are refined with the G3MP2B3 method. All the electronic structure calculations are carried out using the GAUSSIAN 03 program [20].

2.2. The rate constant calculations

The rate constants are evaluated using the conventional transition-state theory (TST) [21,22], the canonical variational transition-state theory (CVT) [23–25],

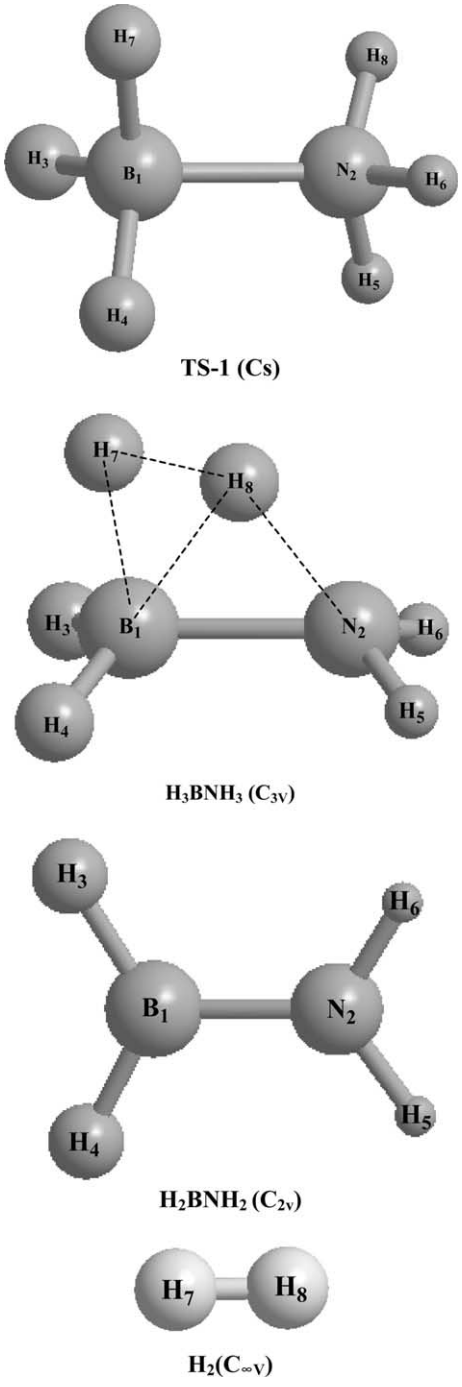

Fig. 1. Pictorial of optimized geometries of the stationary points.

canonical variational transition-state theory with small curvature tunneling correction (CVT/SCT) [26,27], and the TST rate constant calculations [21] with the Eckart tunneling correction (TST/Eckart) [28] by employing the online Vklab program package [29] and POLYRATE 8.2 program [30].

Here, we only give a brief description of the CVT/SCT method. For canonical ensemble at a given temperature T, the canonical variational theory (CVT) thermal rate constant is given by

$$k^{\mathrm{CVT}}(T) = \min_{s} k^{\mathrm{GT}}(T,s)$$

with

$$k^{\mathrm{GT}}(T,s) = \left\{ \sigma \frac{k_{\mathrm{B}}T}{h} \frac{Q^{\mathrm{GT}}(T,s)}{\Phi^{\mathrm{R}}(T)} \mathrm{e}^{-V_{\mathrm{MEP}}(s)/k_{\mathrm{B}}T} \right\},$$

where s is the reaction coordinate. $k^{\mathrm{GT}}(T,s)$ is the generalized transition state theory rate constant at the dividing surface which intersects the MEP at s and is orthogonal to the MEP at the intersection point. σ is the symmetry factor accounting for the possibility of more than one symmetry related reaction path and can be calculated as the ratio of the product of the reactant rotational symmetry numbers to that of the transition state. k_{B} is Boltzman's constant and h is Plank's constant. Q^{GT} is the internal partition function of the generalized transition state with the local zero of energy at $V_{\mathrm{MEP}}(s)$, which is the classical potential energy along the minimum energy path s with its zero of energy at the reactants. Φ^{R} is the reactant partition function per unit volume for bimolecular reactions. Both the Q^{GT} and Φ^{R} are approximated as products of electronic, rotational, and vibrational partition functions. For Φ^{R}, the relative translational partition function is also included. Translational and rotational partition functions are evaluated classically, whereas the vibrational partition functions are calculated quantum mechanically within the harmonic approximation for the present studies.

Furthermore, the CVT rate constants are corrected with the small-curvature tunneling (SCT) [26,27] transmission coefficient. The SCT transmission coefficients, that include the reaction-path curvature effect on the transmission probability, are based on the centrifu-

Table 1
The optimized geometries of reactants, products and transition states at the different levels of theory[a]

Species	Para.	B3LYP/D[a]	B3LYP/AD	B3LYP/T	B3LYP/AT	MP2/D	MP2/AD	MP2/T	MP2/AT	Expt.
H_3BNH_3 (C_{3V})	R(1,2)	1.654	1.657	1.659	1.659	1.657	1.667	1.650	1.651	1.658[b]
	R(1,3)	1.222	1.218	1.207	1.207	1.223	1.220	1.206	1.207	1.216[b]
	R(2,5)	1.023	1.019	1.015	1.015	1.023	1.021	1.013	1.014	1.014[b]
	A(2,1,3)	104.9	104.8	105.0	105.0	104.7	104.5	104.9	104.8	
	A(3,1,4)	113.6	113.7	113.5	113.5	113.8	114.0	113.7	113.7	113.8[b]
	A(1,2,5)	111.7	111.2	111.0	111.0	111.5	111.2	111.0	111.0	
	A(5,2,6)	107.2	107.7	107. 9	107.9	107.3	107.7	107.9	107.9	108.7[b]
TS-1 (Cs)	R(1,2)	1.580	1.587	1.581	1.584	1.592	1.604	1.586	1.591	
	R(1,3)	1.207	1.203	1.192	1.192	1.208	1.205	1.191	1.191	
	R(1,7)	1.392	1.373	1.360	1.356	1.381	1.365	1.349	1.346	
	R(1,8)	1.407	1.396	1.382	1.381	1.400	1.395	1.375	1.376	
	R(2,5)	1.015	1.011	1.006	1.006	1.016	1.013	1.005	1.006	
	R(2,8)	1.390	1.381	1.377	1.373	1.386	1.376	1.368	1.364	
	R(7,8)	0.996	1.002	0.993	0.996	0.981	0.995	0.983	0.989	
	A(2,1,3)	115.1	114.5	114.7	114.5	114.9	114.1	114.4	114.1	
	A(2,1,7)	96.7	97.1	97.3	97.3	96.0	96.3	96.8	96.8	
	A(3,1,4)	119.7	119.8	119.5	119.6	120.1	120.7	120.2	120.5	
	A(3,1,7)	102.6	103.2	103.1	103.3	102.9	103.5	103.3	103.4	
	A(1,2,5)	116.9	117.4	117.7	117.9	115.4	116.8	116.8	117.2	
	A(5,2,6)	111.6	112.2	112.6	112.6	111.4	112.3	112.5	1112.7	
H_2BNH_2 (C_{2v})	R(1,2)	1.389	1.388	1.393	1.390	1.396	1.404	1.392	1.395	1.391[b]
	R(1,3)	1.192	1.192	1.202	1.206	1.207	1.204	1.190	1.191	1.195[b]
	R(2,5)	1.006	1.006	1.011	1.014	1.023	1.012	1.004	1.005	1.004[b]
	A(2,1,3)	119.0	119.0	119.0	119.0	118.9	118.7	118.8	118.8	
	A(3,1,4)	121.9	122.0	122.1	122.0	122.2	122.6	122.4	122.5	122.2[b]
	A(1,2,5)	123.3	123.3	123.3	123.3	123.1	123.0	123.1	123.1	
	A(5,2,6)	113.3	113.4	113.5	113.3	113.8	113.9	113.8	113.7	114.2[b]
H_2 ($C_{\infty v}$)	R(7,8)	0.7617	0.7608	0.7429	0.7429	0.7541	0.7549	0.7372	0.7372	0.741[c]

[a] About the basis sets: cc-pVDZ, aug-cc-pVDZ, cc-pVTZ and aug-cc-pVTZ are abbreviated by D, AD, T and AT, respectively.
[b] Ref. [33].
[c] Ref. [34].

Table 2
Harmonic frequencies (cm^{-1}) and zero point energies (kcal/mol) for the reactants, products and transition states with the different levels of theory

Species	Levels of theory	Harmonic frequencies (cm^{-1})	ZPE
H_3BNH_3 (C_{3V})	B3LYP/cc-pVTZ	259, 645, 650 × 2, 1067 × 2, 1194 × 2, 1195, 1333, 1669 × 2, 2447, 2494 × 2, 3457, 3557 × 2	43.75
	B3LYP/aug-cc-pVTZ	254, 645, 649 × 2, 1065 × 2, 1192 × 2, 1195, 1334, 1668 × 2, 2446, 2493 × 2, 3455, 3553 × 2	43.70
	MP2/cc-pVTZ	270, 687, 649 × 2, 1082 × 2, 1226 × 2, 1217, 1332, 1676 × 2, 2488, 2555 × 2, 3496, 3627 × 2	44.49
	MP2/aug-cc-pVTZ	261, 683, 645 × 2, 1078 × 2, 1218 × 2, 1210, 1329, 1674 × 2, 2480, 2547 × 2, 3485, 3614 × 2	44.32
	Expt.[a]	603, 968, 1301, 1343, 1608, 2340, 2415, 3337, 3386	
TS (C_S)[b]	B3LYP/cc-pVTZ	***1434i***, 360, 573, 734, 866, 1054, 1079, 1097, 1183, 1283, 1307, 1583, 2023, 2124, 2556, 2629, 3575, 3679	39.61
	B3LYP/aug-cc-pVTZ	***1439i***, 357, 571, 732, 858, 1053, 1074, 1096, 1181, 1280, 1313, 1584, 2012, 2129, 2559, 2634, 3575, 3677	39.57
	MP2/cc-pVTZ	***1457i***, 348, 575, 735, 879, 1094, 1095, 1121, 1121, 1328, 1365, 1586, 2090, 2215, 2608, 2692, 3617, 3736	40.45
	MP2/aug-cc-pVTZ	***1466i***, 346, 566, 728, 867, 1086, 1082, 1118, 1197, 1317, 1372, 1591, 2069, 2214, 2605, 2691, 3608, 3726	40.29
H_2BNH_2 (C_{2v})	B3LYP/cc-pVTZ	620, 749, 857, 1015, 1139, 1159, 1363, 1647, 2577, 2651, 3585, 3675	30.08
	B3LYP/aug-cc-pVTZ	622, 748, 852, 1017, 1137, 1156, 1357, 1648, 2578, 2653, 3583, 3670	30.05
	MP2/cc-pVTZ	615, 744, 872, 1029, 1147, 1174, 1379, 1647, 2626, 2710, 3635, 3747	30.49
	MP2/aug-cc-pVTZ	609, 739, 864, 1030, 1140, 1167, 1368, 1649, 2624, 2708, 3623, 3732	30.38
	Expt.[a]	670, 763, 1005, 1131, 1225, 1337, 1625, 2495, 2564, 3451, 3534	
H_2 ($C_{\infty h}$)	B3LYP/cc-pVTZ	4419	6.32
	B3LYP/aug-cc-pVTZ	4418	6.32
	MP2/cc-pVTZ	4524	6.47
	MP2/aug-cc-pVTZ	4522	6.46
	Expt.[c]	4355	

[a] Ref. [31].
[b] There is only an image frequency (shown in the table in bold and italic style) for TS.
[c] Ref. [35].

gal-dominant small curvature semi-classical adiabatic ground-state (CD-SCSAG) approximation. In particular, the transmission probability at energy E is given by

$$P(E) = \frac{1}{\{1 + e^{-2\theta(E)}\}},$$

where $\theta(E)$ is the imaginary action integral evaluated along the reaction coordinate

$$\theta(E) = \frac{2\pi}{h} \int_{s_l}^{s_r} \sqrt{2\mu_{\text{eff}}(s)|E - V_a^G(s)|}\, ds$$

and where the integration limits s_l and s_r are the reaction coordinate classical turning points. The reaction-path curvature effect on the tunneling probability is included in the effective reduced mass μ_{eff}.

3. Results and discussion

3.1. Stationary points

The optimized structures for the stationary points obtained at the B3LYP/aug-cc-pVTZ level of theory are given in Fig. 1. Table 1 lists the optimized geometric parameters of the equilibrium and transition state of the reaction using the B3LYP and MP2 methods with the cc-pVDZ, aug-cc-pVDZ, cc-pVTZ and aug-cc-pVTZ basis sets along with the available experimental data. The optimized geometrical parameters of H_3BNH_3, H_2BNH_2, and H_2 at all the levels of theory employed are in good agreement with the available experimental values [31]. For the transition state, the predicted

Table 3
The reaction energetic parameters (kcal/mol) at different levels of theory

Levels of theory	ΔE	$V^{\neq}$	$V_a^{G\neq}$	$\Delta H^{\circ}_{298\ K}$
B3LYP/cc-pVDZ	−0.42	39.21	35.02	−6.01
B3LYP/aug-cc-pVDZ	−0.25	38.16	34.10	−5.91
B3LYP/cc-pVTZ	−1.73	39.11	34.97	−7.39
B3LYP/aug-cc-pVTZ	−2.09	38.48	34.35	−7.74
MP2/cc-pVDZ	1.68	42.51	38.46	−4.09
MP2/aug-cc-pVDZ	1.25	39.97	36.01	−4.51
MP2/cc-pVTZ	0.98	40.38	36.34	−4.84
MP2/aug-cc-pVTZ	0.52	39.35	35.32	−5.24
E_{HL}//B3LYP/aug-cc-pVTZ	−0.05	40.06	35.93	−5.70
G3			33.09	−7.74
G3MP2			32.95	−8.92
G3MP2B3			32.55	−9.07
CBS-Q			32.47	−8.44
CBS-QB3			32.64	−8.28
Exp.				−5.19 ± 0.48[a]

[a] Ref. [1].

geometries also agree well between all the levels of theory. Table 2 gives the harmonic vibrational frequencies and zero point energies of the equilibrium and transition state structure of the reaction at the B3LYP and MP2 levels of theory along with the previous theoretical results [32] and the available experimental data [31]. The largest relative deviation between our theoretical prediction and experimental measurements is only 8%. Even if for the imaginary frequency of the transition state, the theoretical predictions are quite consistent with each other among the results from different levels of theory. The predicted values of the imaginary frequency are 1434i, 1439i, 1457i, and 1466i cm^{-1} at the B3LYP/cc-pVTZ, B3LYP/aug-cc-pVTZ, MP2/cc-pVTZ, and MP2/aug-cc-pVTZ levels of theory, respectively. This indicates that the shapes of MEP near the transition state among different levels of theory are similar. In the below discussions, only the results for the TS and IRC calculations from the B3LYP/aug-cc-pVTZ level of theory are employed.

Table 3 abstracts the reaction energies (ΔE), the classical potential barriers ($V^{\neq}$), the vibrational adiabatic ground-state potential ($V_a^{G\neq}$) at the transition state, and the theoretical and experimental[1] reaction enthalpies ($\Delta H^{\circ}_{298\ K}$). We can see that all these values are relevant to methods and basis sets employed. Generally, all the values become smaller as the levels of theory and basis sets become higher and larger, respectively. Thus, the combined multi-level methods are required to obtain good estimations of barrier heights and MEP. The largest values of ΔE, $V^{\neq}$, $V_a^{G\neq}$, and $\Delta H^{\circ}_{298\ K}$ are 1.68, 42.51, 38.46, and −4.09 kcal/mol at the MP2/cc-pVDZ level of theory, respectively. The multi-level methods have significant improvement on these energies. In particular, the values of $V_a^{G\neq}$ of multi-level methods (G3, G3MP2, G3MP2B3, CBS-Q and CBS-Q//B3) range from 32.47 to 33.96 kcal/mol, which are much lower than that of single level methods. The multi-level methods are also important to the standard reaction enthalpies ($\Delta H^{\circ}_{298\ K}$). Although the experimental data [1] of $\Delta H^{\circ}_{298\ K}$ (-5.19 ± 0.48 kcal/mol) are larger than the results of multi-level methods (−7.66 to 9.07 kcal/mol), the multi-level methods seem to agree well with each other.

3.2. Reaction path properties

The minimum-energy paths are obtained using the intrinsic reaction coordinate (IRC) theory at the B3LYP/aug-cc-pVTZ level of theory and the potential energy profiles are further refined using the G3MP2B3 method. Fig. 2 shows the variation of selected bond lengths along the minimum energy path of the unimolecular decomposition as a function of reaction coordinate s at the B3LYP/aug-cc-pVTZ level of theory. The B_1–H_3 and N_2–H_5 bonds remain unchanged in the course of the reaction. Along with the increasing of the breaking bond lengths of B_1–H_7 and N_2–H_8 and the decreasing of the bond distances of H_7–H_8, the H_7–H_8 new bonds are formed and the loss of the hydrogen molecule from H_3BNH_3 is completed. The bond length of the breaking bond N_2–H_8 changes more sharply than that of the breaking bond B_1–H_7 during the reaction process, so the eliminations of the hydrogen atoms from the B atom and the N atom are asymmetric, and the B_1–N_2 bond is changed from a single bond (in ammonia borane, H_3BNH_3) to a double bond (aminoborane, H_2BNH_2).

Fig. 3 depicts the vibrationally adiabatic ground-state potential energy curves (V_a^G) of the reaction as a function of s using the refined energies from

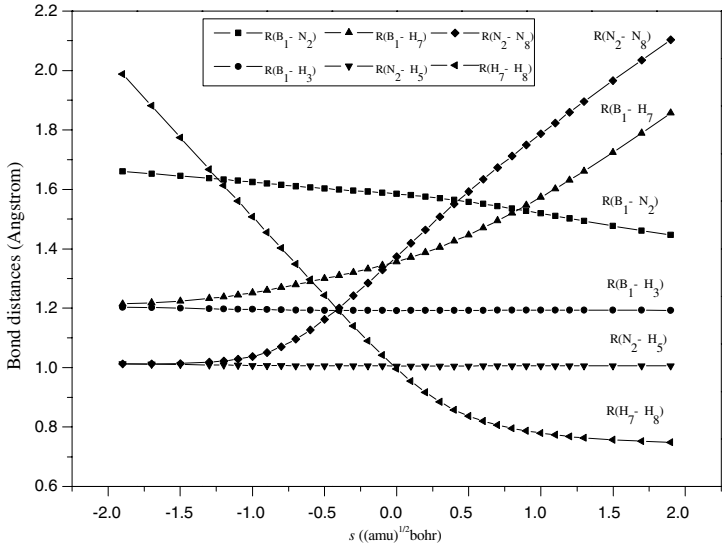

Fig. 2. The changes of bond distances as functions of s $(amu)^{1/2}$ bohr at the B3LYP/aug-cc-pVTZ level of theory.

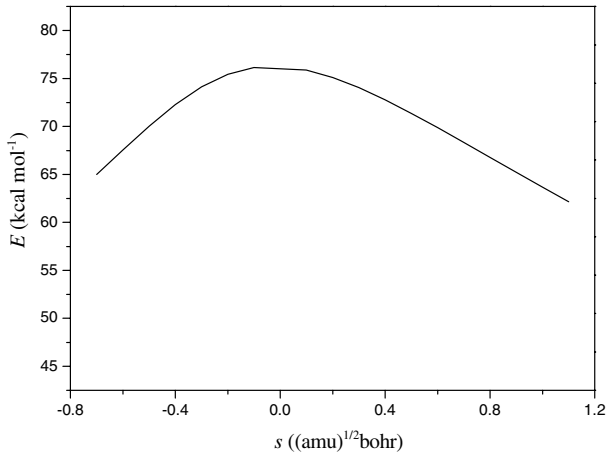

Fig. 3. The vibrationally adiabatic ground-state potential energy curves (V_a^G) of the reaction as a function of s (amu)$^{1/2}$ bohr at the B3LYP/aug-cc-pVTZ level of theory.

G3MP2B3 method based on the B3LYP/aug-cc-pVTZ level of theory. It can be seen that the V_a^G curve is relatively sharp due to its unimolecular reaction nature. This type of reaction is anticipated to have large tunneling effects.

3.3. Rate constant calculations

The rate constants of the title reaction are calculated using the CVT, CVT/SCT, TST, and TST/Eckart methods with the MEP refined at the G3MP2B3 level of theory based on the optimized geometries at the B3LYP/aug-cc-pVTZ levels of theory. The rate constants are shown in Fig. 4. It can be seen that the rate constants calculated at the CVT level are almost identical to those at the TST level over the whole temperature range. This implies that the variational effect of the reaction is small. As discussed in the previous section that the shape of MEP of the reaction is sharp and this may result in a large tunneling effect at low temperatures. We can see that at temperatures below 500 K, the rate constants of CVT/SCT are remarkably larger than those of CVT. At 200 K, the CVT/SCT rate constants are about 6 orders of magnitude larger than the CVT rate constants. The Eckart method is a good approximation of tunneling effect for the title reaction. Thus, the TST/Eckart rate constant is close to the CVT/SCT rate constants. The fitted Arrhenius expression calculated from CVT/SCT method is $k(T) = 6.86 \times 10^6 \times T^{1.69} \times e^{(-1.37\times10^4/T)}$ s^{-1}. The apparent activation energy in this expression is 27.2 kcal/mol, which is in accordance with the experiments result that the reaction proceeds at relatively low temperatures (410 K).

4. Summary

In the present study, a direct dynamics study of thermal rate constants of the H_2 elimination reaction from ammonia borane (H_3BNH_3) has been carried out employing the B3LYP and ab initio methods. The geometries and harmonic vibrational frequencies of all the stationary points are calculated by means of B3LYP and MP2 with cc-pVDZ, aug-cc-pVDZ, cc-pVTZ and aug-cc-pVTZ basis sets. The information along the minimum energy potential is carried out at B3LYP/aug-cc-pVTZ. The energies and enthalpies are refined using the G3, G3MP2, G3MP2B3, CBS-Q,

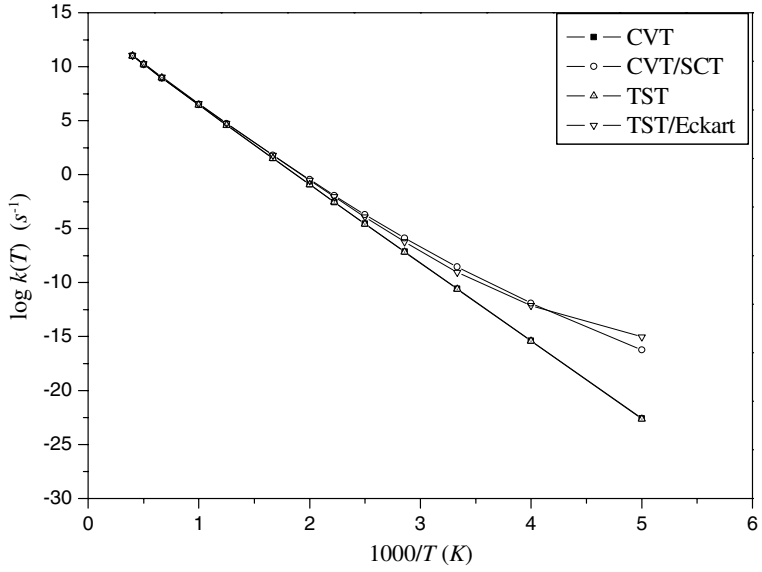

Fig. 4. Arrhenius plot of the rate constants calculated at the CVT, CVT/SCT, TST and TST/Eckart levels of theory. The rate constants are calculated based on the interpolated MEP at the B3LYP/aug-cc-pVTZ level of theory.

CBS-Q//B3, and Martin's high-level method based on the geometries optimized using B3LYP/aug-cc-pVTZ level of theory. The rate constants of the reaction are calculated by using the TST, CVT, CVT/SCT, and TST/Eckart methods.

Acknowledgments

Our thanks are due to D.G. Truhlar for providing the POLYRATE 8.2 program. This work is supported by the National Natural Science Foundation of China (No. 20373007 and No. 20471008) and the Foundation for basic research by the Beijing Institute of Technology.

References

[1] G. Wolf, J. Baumann, F. Baitalow, F.P. Hoffmann, Thermochim. Acta 343 (2000) 19.
[2] F. Baitalow, J. Baumann, G. Wolf, K. Jaenicke-Rlobler, G. Leitner, Thermochim. Acta 391 (2002) 159.
[3] R.A. Geanangel, W.W. Wendlandt, Thermochim. Acta 86 (1985) 375.
[4] V. Sit, R.A. Geanangel, W.W. Wendlandt, Thermochim. Acta 113 (1987) 379.
[5] G. Wolf, J.C. van Miltenburg, U. Wolf, Thermochim. Acta 317 (1998) 111.
[6] J.S. Wang, R.A. Geanangel, Inorg. Chim. Acta 148 (1988) 185.
[7] D.G. Truhlar, M.S. Gordon, Science 249 (1990) 491.
[8] T.H. Dunning Jr., J. Chem. Phys. 90 (1989) 1007.
[9] A.D. Becke, J. Chem. Phys. 104 (1996) 1040.
[10] C. Lee, W. Yang, R.G. Parr, Phys. Rev. B 37 (1988) 785.
[11] L.A. Curtiss, K. Raghavachari, P.C. Redfern, V. Rassolov, J.A. Pople, J. Chem. Phys. 109 (1998) 7764.
[12] L.A. Curtiss, P.C. Redfern, K. Raghavachari, V. Rassolov, J.A. Pople, J. Chem. Phys. 110 (1999) 4703.
[13] A.G. Baboul, L.A. Curtiss, P.C. Redfern, K. Raghavachari, J. Chem. Phys. 110 (1999) 7650.
[14] J.W. Ochterski, G.A. Petersson, J.A. Montgomery Jr., J. Chem. Phys. 104 (1996) 2598.
[15] J.A. Montgomery Jr., M.J. Frisch, J.W. Ochterski, G.A. Petersson, J. Chem. Phys. 112 (2000) 6532.
[16] J.M.L. Martin, Chem. Phys. Lett. 256 (1996) 669.
[17] J.A. Pople, M. Head-Gordon, K. Raghavachari, J. Chem. Phys 87 (1987) 5968.
[18] M.J. Frisch, M. Head-Gordon, J.A. Pople, Chem. Phys. Lett. 166 (1990) 275.
[19] C. Gonzalez, H.B. Schlegel, J. Chem. Phys. 90 (1989) 2154.
[20] M.J. Frisch et al., GAUSSIAN 98, Gaussian Inc., Pittsburgh, PA, 1998.
[21] D.G. Truhlar, A.D. Isaacson, B.C. Garrett, in: M. Bacr (Ed.), Theory of Chemical Reaction Dynamics, vol. 4, CRC Press, Boca Raton, FL, 1985.
[22] D.G. Truhlar, B.C. Garrett, Acc. Chem. Res. 13 (1980) 440.
[23] N.T. Truong, J. Chem. Phys. 100 (1994) 8014.
[24] W.H. Miller, J. Am. Chem. Soc. 101 (1979) 6810.
[25] D.G. Truhlar, B.C. Garrett, Annu. Rev. Phys. Chem. 35 (1984) 159.
[26] Y.-P. Liu, G.C. Lynch, T.N. Troung, D.-H. Lu, D.G. Truhlar, B.C. Garrett, J. Am. Chem. Soc. 115 (1993) 2408.
[27] D.G. Truhlar, A.D. Isaacson, R.T. Skodje, B.C. Garrett, J. Phys. Chem. 86 (1982) 2252.
[28] N.T. Truong, D.G. Truhlar, J. Chem. Phys. 93 (1990) 1761.
[29] S.-W. Zhang, T.N. Truong, VKLab version 1.0, University of Utah, 2001.
[30] Y.Y. Chuang, J.C. Corchado, P.L. Fast, J. Vill, W.-P. Hu, Y.-P. Liu, G.C. Lynch, C.F. Jackels, K.A. Nguyen, M.Z. Gu, I. Rossi, E.L. Isaacson, D.G. Truhlar, POLYRATE, Program vision 8.2, Minneapolis, 1999.
[31] P. Brint, B. Sangchakr, P.W. Fowler, J. Chem. Soc., Faraday Trans. II 85 (1989) 29.
[32] M.L. McKee, J. Phys. Chem. 96 (1992) 5380.
[33] J.M. Sugie, H. Takeo, C. Matsumure, Chem. Phys. Lett. 64 (1979) 573.
[34] G.W.C. Kaye, T.H. Laby, Tables of Physical and Chemical Constants, Longman Group Limited, 1995.
[35] N.L. Ira, Molecular Spectroscopy, Wiley, New York, 1975.